Annals of Biomedical Engineering, Vol. 35, No. 3, March 2007 *(© 2007)* pp. 321–336
DOI: 10.1007/s10439-006-9234-1

Incorporation of Myofilament Activation Mechanics into a Lumped Model of the Human Heart

DIMITRI DESERRANNO,[1,2] MOHAMMAD KASSEMI,[1] and JAMES D. THOMAS[2]

[1]National Center for Space Exploration Research, NASA Glenn Research Center, 21000 Brookpark Rd MS 110-3, Cleveland, OH 44135, USA and [2]Cleveland Clinic Foundation, 9500 Euclid Ave F15, Cleveland, OH 44195, USA

(Received 14 January 2006; accepted 14 November 2006; published online 12 January 2007)

Abstract—The success and usefulness of lumped cardiovascular models are directly dependent on the physiological fidelity of their formulation. In most existing lumped formulations for the heart, the compliance of the chamber is modeled based on its electrical analog, the capacitor. This has traditionally resulted in the use of a pre-described time-varying stiffness modulus for simulating the cardiac contractions. Unfortunately, such a time-varying stiffness does not include any physiological contractile machinery and thus no dependency on fiber sarcomere length and intracellular calcium concentrations, key mechanisms responsible for proper cardiac function. In this paper a lumped cardiovascular model is presented that is based on the incorporation of detailed myofilament activation for simulating the ventricular calcium binding and crossbridging mechanism. Upon validation against experimental data, it is shown that the new myofilament activation-based model considerably increases the physiological validity and internal consistency of the cardiovascular simulations in comparison to the traditional variable compliance-based models. It is also shown, through specific case studies, that the present model can serve as a quick response tool for testing various hypotheses concerning the impact of the calcium binding and crossbridge kinetics on the overall performance of the cardiovascular system.

Keywords—Lumped parameter model, Actin–myosin, Calcium binding, Myofilament activation, Heart, Cardiovascular system.

INTRODUCTION

A proper computational hemodynamic assessment of either the heart or the circulatory system requires information on both systems. In general, the circulatory system constitutes as an afterload for the heart while the heart acts as a preload for the vessel.[37] If this functional coupling is properly reflected by the mathematical formulations for each system then it allows independent changes in the state variables of both models. Thus, a functional physiological prediction of one model facilitates a physiologically valid prediction of the other. The heart is usually modeled using a time-variant elastance concept expressed as a pressure–volume relationship. The vascular system has been typically represented by various types of the so-called Windkessel lumped parameter models.

Although finite element or finite volume continuum models can undoubtedly provide more detailed information with regard to the spatial variations of pressure, velocity, stress and strain within the different cardiovascular domains, they inevitably carry a large computational burden and from a practical point of view are only suited for single organ modeling and analysis. Lumped parameter models, however, can provide an integrated analysis of the entire cardiovascular system with considerable computational efficiency.

A major difficulty in using a lumped system model as an effective clinical or research tool is the need to extract numerous model parameters from measurements of arterial blood flow and pressure.[19] This problem is often cited as the most important impediment to broader use and application of the lumped model approach.[10,15] Despite of this difficulty, lumped parameter models have been applied to improve our understanding of the cardiovascular system response to internal or external perturbations brought about by disease or disorder with a considerable degree of success.

In the 1990s Thomas developed a model of the entire cardiovascular system, consisting of eight compartments, leading to 24 coupled first-order differential equations.[31] It was used to discern determinants of pulmonary vein flow, mitral regurgitation, prolongation of the mitral deceleration time, mitral stenosis and the impact of disease on transmitral flow.[4,5,13,32,33] Recently, it was used to simulate the sensitivity of left

Address correspondence to Dimitri Deserranno, National Center for Space Exploration Research, NASA Glenn Research Center, 21000 Brookpark Rd MS 110-3, Cleveland, OH 44135, USA. Electronic mail: dimitri.deserranno@gmail.com

ventricle (LV) contractility to the acceleration of the aortic flow.[1] It also demonstrated that single-beat estimates of contractility are sensitive to preload, ventricular size, and presence of mitral regurgitation,[23] and that prolonged treatment with sodium nitroprusside in patients with aortic stenosis results in a change of systolic properties of the left ventricle.[22]

There has been a considerable amount of activity in the area of lumped model. The list of researchers applying lumped models is simply never ending. Models that have been applied to study cardiovascular responses to tilt, lower body negative pressures, and orthostatic stress have become increasingly complex, including a 14-compartment cardiovascular system by Heldt and a 28-compartment model by Peterson and Croston.[8–10,21] Wijkstra and Boom analyzed ventricular deactivation during constant ejection in 1989.[35] In 1993 Ye *et al.* added vessel taper into a vascular lumped model,[36] and Soans *et al.* simulated variable area diastolic filling in 2002.[30]. Ventricular wall stress normalization by Segers *et al.*[28] and the impact of variable gravity by Schroeder *et al.*[27], White[34] and Heldt *et al.*[8] are examples of investigations into cardiac behavior under altered physiological conditions. The chick vascular system was even modeled by Yoshigi *et al.*[37] Finally, the lumped models have been extended and used to study the cerebral blood flow regulation[20] as well as the interaction with the pulmonary and baroreflex systems.[14]

The success and usefulness of these lumped cardiovascular models is directly dependent on the physiological fidelity of its formulation. Traditionally, lumped models have been developed based on either abstract electrical circuit analogs or purely fluid mechanics-based mathematical derivations.[8–10,14,19,21,32] Unfortunately, both of these approaches may depart significantly from the underlying physical and physiological realities of the cardiovascular system and whenever this occurs problems arise. In this paper, we will address a rather significant limitation in simulating contractile ventricular function through the use of the empirically based time-varying modulus of elasticity. This approach specifies *a priori* a specific structural behavior and lacks any physiologically valid myofilament activation kinetics, that depends on fiber sarcomere length and intracellular calcium concentration, key pathways responsible for realistic cardiac function. To alleviate this shortcoming we will incorporate a comprehensive myofilament activation model into the lumped cardiovascular model presented here. The resulting cardiovascular model is verified and validated against benchmark experimental and clinical *in vivo* data. We will also show, through specific case studies, that incorporation of the calcium binding and crossbridging mechanisms into the present lumped cardiovascular model not only enhances its physiological fidelity in comparison to existing lumped cardiovascular models in the literature, but also produces a quick response numerical modeling tool that can be used to examine and test various hypotheses.

MATHEMATICAL FORMULATION

The lumped cardiovascular model is based on a "0"-order mathematical representation of four cardiac chambers and four vascular chambers as shown in Fig. 1. The compartments consist of the following: pulmonary veins (PV), left atrium (LA), left ventricle (LV), systemic arteries (SA), systemic veins (SV), right atrium (RA), right ventricle (RV) and pulmonary arteries (PA). These compartments are inter-connected through the following flow nodes: left atrial inlet (LAI), mitral valve (MV), aortic valve (and main systemic artery) (AV), systemic capillaries (SC), right atrial inlet (RAI), tricuspid valve (TV), pulmonic valve (and main pulmonary artery) (PV) and pulmonary capillaries (PC). As a result each chamber, represented by a pressure and a volume, is flanked by two flow nodes on either side.

Lumped Fluid Mechanics

The vascular model is adopted from Thomas *et al.*[32] Briefly, a first-order differential equation at each flow

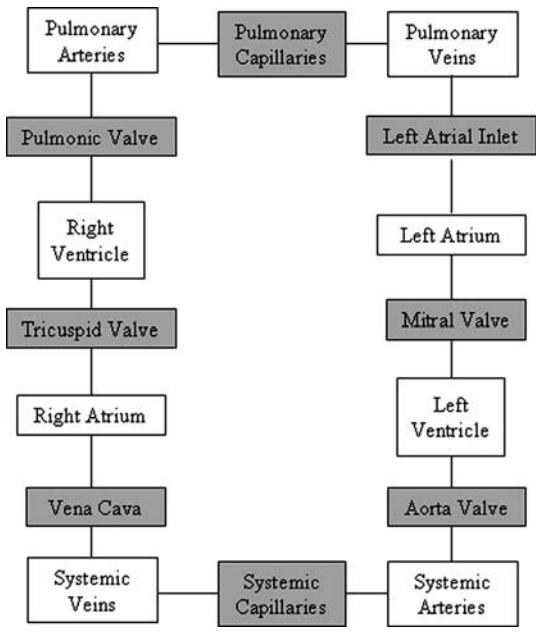

FIGURE 1. The lumped model shown above illustrates the closed loop cardiocirculatory system (white: Lumped chamber, Gray: Lumped flow node).

TABLE 1. Summary of cardiac flow lumped parameters.

	Mitral valve	Aortic valve (and arteries)	Tricuspid valve	Pulmonic valve (and arteries)
m (mmHg s^2/cm^3)	1.25	17	1.25	5
A (cm^2)	4	4	4	4
R_1 (mmHg s/cm^3 (forward))	0	15	0	30
R_1 (mmHg s/cm^3 (reverse))	10^6	10^6	10^6	10^6
R_2 ([])	1.0	0	1.0	0

node describes the relationship between the inter-chamber flow rates and pressure difference. Certain flow nodes will only allow forward flow (heart valves), while others enable flow in both directions (vessels).

The change in flow rate at a given node, represented by Q_i, can be computed from the following expression:

$$\frac{dQ_i}{dt} = \frac{P_{\text{upstream}} - P_{\text{downstream}} - R_1(Q) - R_2(Q)}{m} \quad (1)$$

where $R_1(Q)$ and $R_2(Q)$ are the linear and quadratic resistance terms, respectively, and m is the flow inertia (Tables 1 and 2).

The resistance term $R_1(Q)$ represents the contributions to the overall pressure drop by the viscous friction of a laminar flow typically found in vessels, and is simply given as a linear function of flow rate:

$$R_1(Q) = R_1 \cdot Q \quad (2)$$

While the resistance term $R_2(Q)$ represents the pressure drop caused by flow obstructions such as the valves, for example, and are given as a fraction of the dynamic pressure:

$$R_2(Q) = R_2 \cdot \frac{1}{2}\rho\left(\frac{Q}{A}\right)^2 \quad (3)$$

where A is the effective cross-sectional area of the flow, and ρ the fluid density, set to 1.05 g/cm^3. Note that R_1 has the units of kg/m^{4}s, while R_2 is dimensionless.

These equations allow for both forward and reverse flows, thus reducing the number and complexity of the ODE's describing the circulation. The potential for reverse flows at heart valves is minimized by assigning a rather large resistance value R. As a result, in our simulations the maximum reverse valvular flow observed was about 0.1 ml/s, compared to the maximum forward valvular flow of about 500 ml/s.

TABLE 2. Summary of vascular flow lumped parameters.

	Left atrial inlet	Systemic capillaries	Right atrial inlet	Pulmonary capillaries
m (mmHg s^2/cm^3)	3	10	3	5
R_1 (mmHg s/cm^3)	140	1200	120	200
R_2 ([])	0	0	0	0

Lumped Solid Mechanics

Each chamber is described by a volume, which depends on the flow rates of the adjacent flow nodes using a simple ordinary differential equation:

$$\frac{dV_i}{dt} = Q_{\text{upstream}} - Q_{\text{downstream}} \quad (4)$$

To provide a well-defined system of equations, chamber pressures and volumes must be mathematically linked. Different approaches are taken for the vascular chambers, atria and ventricles as described next.

Vascular Chambers

The pressure and volume of the vascular chambers are related through a single compliance value, such that:

$$P(V) = \frac{V - V_0}{C} \quad (5)$$

where C is the chamber compliance and V_0 is the chamber resting volume at zero pressure (Table 3).

Heart Atria

The pressure–volume relationships of the atria are represented by the following nonlinear expressions:

$$P(V) = P_{\text{p}}(V) + P_{\text{a}}(V) \quad (6)$$

where $P_{\text{p}}(V)$ and $P_{\text{a}}(V)$ respectively represent the passive and active contribution of muscle stiffness to pressure. Note that during contraction, the passive tissue stiffness never physically disappears. Any inherent elastic stiffness of the heart is present during both diastolic and systolic analysis, therefore the passive term is always present in contrast to earlier works.[4–6,8–10,13,21,32,33]

The passive nonlinear elastic contribution to the chamber pressure is modeled using an approach similar to Thomas *et al.*[32]:

TABLE 3. Summary of vascular compartment lumped parameters.

	Systemic arteries	Systemic veins	Pulmonary arteries	Pulmonary veins
C (cm^3/mmHg)	1.2	35	3.5	15
V_0 (cm^3/mmHg	300	3200	120	300

TABLE 4. Summary of cardiac compartment lumped parameters.

	Left ventricle	Right ventricle	Left atrium	Right atrium
V_0 (cm^3)	35	35	30	30
P_{d0} (mmHg)	0	0	0	0
V_{min} (cm^3)	10	10	10	10
P_{min} (mmHg)	−5	−5	−5	−5
V_{k+} (cm^3)	60	65	60	60
E_{d0} (mmHg/cm^3)	0.09	0.06	0.07	0.07
Ca_{max} (μM)	0.7	0.5	N/A	N/A
t (s)	0.10	0.10	N/A	N/A
$P_{systole}$ (mmHg)	410	300	N/A	N/A
E_s (mmHg/cm^3)	N/A	N/A	0.19	0.19
V_{s0} (cm^3)	N/A	N/A	20	20
t_{act} (s)	N/A	N/A	0.14	0.14

$$\begin{aligned} P_{\mathrm{p}}(V) &= P_{0^+} e^{\frac{V-V_0}{V_{k^+}}} + P_{b^+} \quad \text{when } V \geq V_0 \\ &= P_{b^-} - P_{0^-} e^{\frac{V_0-V}{V_{k^-}}} \quad \text{when } V \leq V_0 \end{aligned} \tag{7}$$

Here $P_{0^+}, P_{0^-}, P_{b^+}, P_{b^-}, V_{k^-}, V_{k^+}$ describe the nonlinear relationship between pressure and volume. The P-parameters are computed based on the value, P_{d0}, and slope, E_{d0}, at the volume V_0, rendering a system of four equations with four unknowns. The value of V_{k^-} is computed based on the minimum pressure and volume, while V_{k^+} is prescribed directly (Table 4).

Atrial contraction is modeled as a raised cosine[32]:

$$P_{\mathrm{a}}(V) = \frac{1}{2}\left(1 - \cos\left(\frac{2\pi t}{t_{\mathrm{act}}}\right)\right) \cdot E_{\mathrm{systole}} \cdot (V - V_{s0}) \tag{8}$$

where t_{act}, $E_{systole}$ and V_{s0} are the model parameters.

Heart Ventricles

Similarly to the atria, the pressure–volume relationships of the ventricles are represented by the nonlinear expressions of Eqs. (6) and (7) with the ventricular parameters summarized in Table 4. While in the past, a single algebraic equation was used to model systolic pressure through a time-varying elastance, the active contribution to ventricular pressure in this model is computed through a lumped actin–myosin crossbridging and calcium binding model based on the earlier work of Rice *et al.*[25] using the following expressions:

A calcium transient model: Since cardiac electrophysiology is out of the scope of the present work, calcium transience will be considered as an input to the lumped ventricular model. The calcium transient input is based on the Luo–Rudy (LRd) model for a single cardiac cell.[3,26,29] Using a nonlinear curve fit, an analytical representation is developed for the calcium transient as represented by the temporal behavior of Ca_i, shown in Fig. 2. The input parameters considered include: the heart rate hr, the rate of calcium release τ_{act}, the maximum calcium level Ca_{max}, the duration of calcium release Ca_{dur}, the rate of calcium uptake τ_{deact}, and the minimum calcium level Ca_{min} (Table 5). It was found that a piecewise function of 2 sigmoids, 1 parabola and 1 linear curve provided the desired accuracy (r = 0.995, S.E. = 0.08%). The resulting equations describing the parameterized calcium profile are:

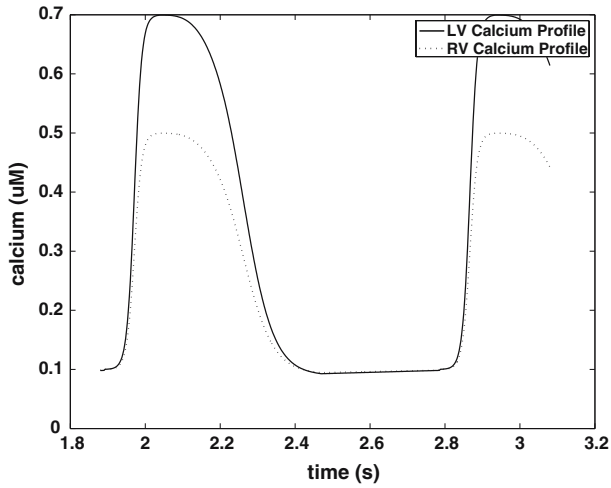

FIGURE 2. Calcium transient profile applied as input to the myofilament activation model.

$$\begin{aligned} t_0 &= \mathrm{modulo}(t, 60/hr) \\ t_1 &= t_0 + 7.0\tau_{\mathrm{act}} \\ t_2 &= t_0 + \mathrm{Ca}_{\mathrm{dur}} - 1.35\tau_{\mathrm{act}} \\ t_3 &= 2\mathrm{Ca}_{\mathrm{dur}} \\ \mathrm{Ca}_i &= \mathrm{Ca}_{\mathrm{min}} + \frac{\mathrm{Ca}_{\mathrm{max}} - \mathrm{Ca}_{\mathrm{min}}}{1+\exp(-\frac{t-t_0}{\tau_{\mathrm{act}}})} \quad (t_0 < t < t_1) \\ \mathrm{Ca}_i &= \mathrm{Ca}_{\mathrm{max}} - A * (t - t_1)^B \quad (t_1 < t < t_2) \\ \mathrm{Ca}_i &= 0.985\mathrm{Ca}_{\mathrm{max}} - \frac{\mathrm{Ca}_{\mathrm{max}} - \mathrm{Ca}_{\mathrm{min}}}{1+\exp(-\frac{t-t_0-\mathrm{Ca}_{\mathrm{dur}}}{\tau_{\mathrm{deact}}})} \quad (t_2 < t < t_3) \\ \mathrm{Ca}_i &= \mathrm{Ca}_{\mathrm{min}} \quad (t_3 < t) \end{aligned} \tag{9}$$

where A and B are computed to provide a zero- and first-order continuous function at time t_2.

A calcium binding model: The calcium binding model is described by the sketch in Fig. 3 and consists of two states in which troponin is either bound or not bound to calcium,[24,25] depending on the free calcium concentration as described by the calcium transient in Eq. (9). The calcium binding model can be reduced to a

TABLE 5. Summary of calcium transient parameters.

	Ca_{max} (μM)	Ca_{min} (μM)	τ_{act} (ms)	τ_{deact} (ms)	Ca_{dur} (ms)
Left ventricle	0.7	0.1	10	40	290
Right ventricle	0.5	0.1	10	40	290

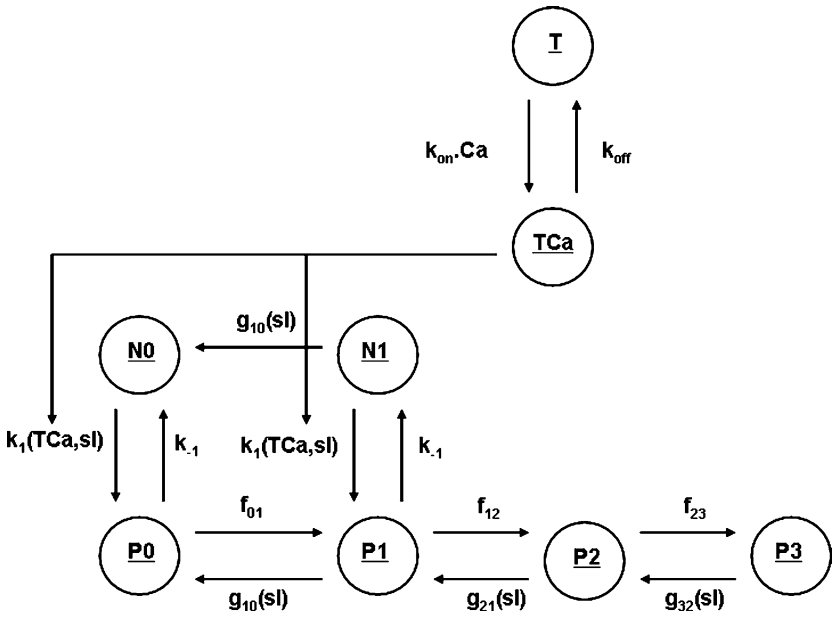

FIGURE 3. The myofilament activation model includes a calcium binding and crossbridge model as developed by Rice *et al.*[25] T-TCa: unbound and bound troponin. N-P: nonpermissive and permissive crossbridge states. 0–3: number of attached crossbridges.

single first order ordinary differential equation, describing the binding of calcium to troponin:

$$\frac{d\mathrm{TCa}}{dt} = k_{\mathrm{on}}\mathrm{Ca}_i(1-\mathrm{TCa}) - k_{\mathrm{off}}\mathrm{TCa} \qquad (10)$$

where k_{on} and k_{off} are model parameters.

An actin–myosin crossbridging model: The crossbridge kinetics model consists of six states (2 nonpermissive states with 0 or 1 attached crossbridge: N_0, N_1 and 4 permissive states with 0–3 attached crossbridges: P_0, P_1, P_2 and P_3), depending on both the troponin–calcium complex, TCa, and the sarcomere length, SL, as shown in Fig. 3 and described in detail by Rice *et al.*[25] The crossbridge kinetics model is based on six coupled first-order ordinary differential equations:

$$\begin{aligned}
\frac{dN_0}{dt} &= g_{10}N_1 + k_{-1}P_0 - k_1N_0\\
\frac{dN_1}{dt} &= k_{-1}P_1 - (k_1+g_{10})N_1\\
\frac{dP_0}{dt} &= k_1N_0 + g_{10}P_1 - (f_{01}+k_{-1})P_0\\
\frac{dP_1}{dt} &= k_1N_1 + f_{01}P_0 + g_{21}P_2 - (f_{12}+g_{10}+k_{-1})P_1\\
\frac{dP_2}{dt} &= f_{12}P_1 + g_{32}P_3 - (f_{23}+g_{21})P_0\\
\frac{dP_3}{dt} &= f_{23}P_2 - g_{32}P_3
\end{aligned} \qquad (11)$$

The rate constants f_{ij}, g_{ji}, and k_i in the crossbridge dynamics model are computed based on the sarcomere length, the amount of troponin-bound calcium and several constants as shown in Table 6.

A force-generating model: Once the individual states of the myofilament activation model are computed, the normalized force generated by the sarcomeres can be determined by adding the strongly bound crossbridge states taking into account the number of interactions with each functional state[25]:

$$F_{\mathrm{norm}} = \alpha\frac{P_1 + N_1 + 2P_2 + 3P_3}{F_{\mathrm{max}}} \qquad (12)$$

Here α is a parameter between 0 and 1 that takes into account the amount of overlap between thick and thin filaments based on the sarcomere length (see Fig.4). This parameter can be computed as follows:

TABLE 6. Summary of myofilament activation parameters.

$\mathrm{SL}_{\mathrm{ref}}$	1.85
SL	$\mathrm{SL}_{\mathrm{ref}} \cdot \left(\frac{V}{V_0}\right)^{\frac{1}{7.7}}$
$\mathrm{SL}_{\mathrm{norm}}$	$\frac{\mathrm{SL}-1.65}{2.35-1.65}$
k_{on}	$36\cdot\mathrm{Ca}_i$
k_{off}	18
$K_{1/2}$	$\left(1+\frac{k_{\mathrm{on}}/k_{\mathrm{off}}}{0.5+(1.0-\mathrm{SL}_{\mathrm{norm}})^{1.6}}\right)^{-1}$
k_{-1}	42
k_{+1}	$31.5 * \left(\frac{\mathrm{TCa}}{K_{1/2}}\right)^{5+3.0\cdot\mathrm{SL}_{\mathrm{norm}}}$
f	9
f_{01}	$3f$
f_{12}	$14f$
f_{23}	$10f$
g	$k_{-1}\left(1+4.0\cdot(1.0-\mathrm{SL}_{\mathrm{norm}})^{4.0}\right)$
g_{10}	g
g_{21}	$2g$
g_{32}	$3g$

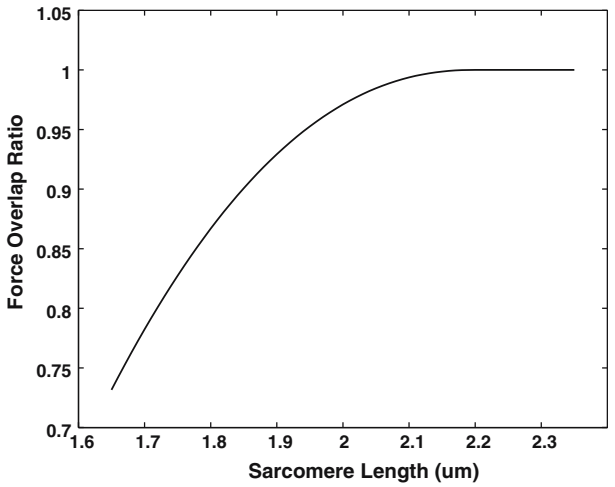

FIGURE 4. Overlap ratio α as a function of sarcomere length required in Eq. (13).

$$\alpha = 1.0 - (2.2 - \mathrm{SL})^{2.2} \quad \text{when SL} \leq 2.2$$
$$\alpha = 1.0 \quad \text{when SL} \geq 2.2$$

The original description of α as published[25] has a discontinuity in the derivative of the force. Here, this discontinuity is removed while closely representing the original functional relationship ($r = 0.993$).

The normalization factor $F_{\max}$ from Eq. (12) is[25]:

$$\begin{aligned} F_{\max} &= P_{1,\max} + 2P_{2,\max} + 3P_{3,\max} \\ P_{1,\max} &= \frac{f_{01}g_{21}g_{32}}{\sum} \\ P_{2,\max} &= \frac{f_{01}f_{12}g_{32}}{\sum} \\ P_{3,\max} &= \frac{f_{01}f_{12}f_{23}}{\sum} \\ \sum &= f_{01}g_{21}g_{32} + f_{01}f_{12}g_{32} + f_{01}f_{12}f_{23} + g_{10}g_{21}g_{32} \end{aligned} \tag{14}$$

5. A pressure–force coupling model: The following equation links the fiber forces to the active ventricular pressure contribution:

$$P_s(v) = F_{\text{norm}} \cdot P_{\text{systole}} \cdot \left(\frac{V}{V_0}\right)^{\frac{1}{2}} \tag{15}$$

where P_{systole} is the absolute maximum developed pressure ($F_{\text{norm}} = 1$), and V_0 is the volume at zero pressure.

Boundary Conditions

No boundary conditions are needed to solve this system since the lumped computational domain renders a spatially closed loop system that evolves in time (Fig.1). The system of ODEs that form the basis of our cardiovascular model is given by the following recursive expression:

$$\begin{aligned} \frac{dV_i}{dt} &= Q_{\text{upstream}} - Q_{\text{downstream}} \\ \frac{dQ_i}{dt} &= \frac{P_{\text{upstream}} - P_{\text{downstream}} - R_1(Q_i) - R_2(Q_i)}{m} \\ P_i &= P_{\text{passive}}(V_i) + P_{\text{active}}(V_i, \text{Ca}) \end{aligned} \tag{16}$$

This system of equations were solved using the stiff ODE solver "ode23tb" in Matlab 6 (Mathworks Inc., Natick, MA). The data was sampled every 2.5 ms.

Initial Conditions

In the cases presented here, the lumped model is first started in an unphysiological state of zero flow. The pressures are chosen such that the initial volume stored in the entire system is approximately 5000 ml, roughly equal to the total human blood volume. The selected initial pressure values were as follows: left atrium (5 mmHg), left ventricle (0 mmHg), systemic arteries (100 mmHg), systemic veins (15 mmHg), right atrium (5 mmHg), right ventricle (0 mmHg), pulmonary arteries (20 mmHg) and pulmonary veins (10 mmHg). In addition, the initial fibers states were set to zero, except N_0 that was set to 1. In this fashion the requirement that the sum of all the states needs to equal 1 at all times is satisfied. Starting with this set of initial conditions the system was subsequently marched through 20 or more cardiac cycles to bring the simulation to a physiologically acceptable state of operation, thus removing the direct impact of the original, arbitrarily selected initial conditions.

NUMERICAL EXPERIMENTS

The degree of success of any lumped model in predicting a physiologically realistic behavior for the cardiovascular system is largely dependent on the proper identification of the numerous model parameters that must be specified. In this work we have extracted initial guesses of the pertinent model parameters from previous publications.[25,32] The optimal parameter values were estimated through systematic sensitivity analysis during three numerical experiments: (1) simulating the force–calcium relations of the fibers at various stretches, (2) simulating preload and afterload through aortic occlusion and bleeding at two levels of contractility, and (3) benchmarking the results against experimental clinical data obtained at the Cleveland Clinic Foundation. After presenting our model validation and verification results, we will

discuss some details of the simulated behavior of the most pertinent cardiovascular variables under baseline conditions.

The cardiac and vascular flow parameters are summarized in Tables 1 and 2, respectively. The cardiac and vascular compartments parameters are summarized in Tables 3 and 4, respectively. The default parameter values for the calcium transients of the left and right ventricles in large mammals can be found in Table 5. The parameters describing the dynamic behavior of a contracting heart through the myofilament activation of the ventricles are given in Table 6.

Numerical Experiment 1: Force–Calcium Relationships for the Contractile Fibers

The force–calcium relationships at various sarcomere lengths computed by the myofilament activation model is graphically represented in Fig. 5. Here the steady state normalized fiber force (Eq. 12) is plotted against intracellular calcium concentration over the entire range of physiological sarcomere lengths. As shown, the force increases quickly from its minimum to its maximum value when intracellular calcium concentrations increase from 0.2 to 0.9 μM. Additionally, as expected, shorter sarcomeres develop less force when activated due to the reduced overlap ratio α and force generating rate k_{+1}, and the increased force deactivation rate g. The modeled behavior is in agreement with previous work.[12,25]

Numerical Experiment 2: Ventricular Preload and Afterload Variations

The response of the ventricular model to changes in afterload (A) and preload (B) is shown in Fig. 6. Here afterload is altered by the occlusion of the systemic artery, while preload variations are obtained through bleeding in the systemic veins. Contractility is computed as the maximum pressure/volume ratio and reported in Fig. 6. Increasing the occlusion shifts the pressure–volume loop to the right, rendering an increase in the volume and pressure. Similarly, increasing bleeding shifts the pressure–volume loop to the left, reducing the ventricular volume and pressure. The downward bend of these relationships at lower volumes is consistent with previously observed clinical behavior.[2,11] The experiment is also repeated for a 10% increase in calcium concentration to demonstrate the increase in contractility, observed by the shift of the curve to the left and up. Additionally, as reported earlier, the curvature increases as contractility increases.[2,11]

Numerical Experiment 3: Validation Against In Vivo Clinical Data

The validation tests were based on available experimental/clinical cardiovascular data gathered from a total of 12 normal volunteers at the Cleveland Clinic Foundation as published by Notomi *et al.*[17] The protocol was approved by the institutional review board

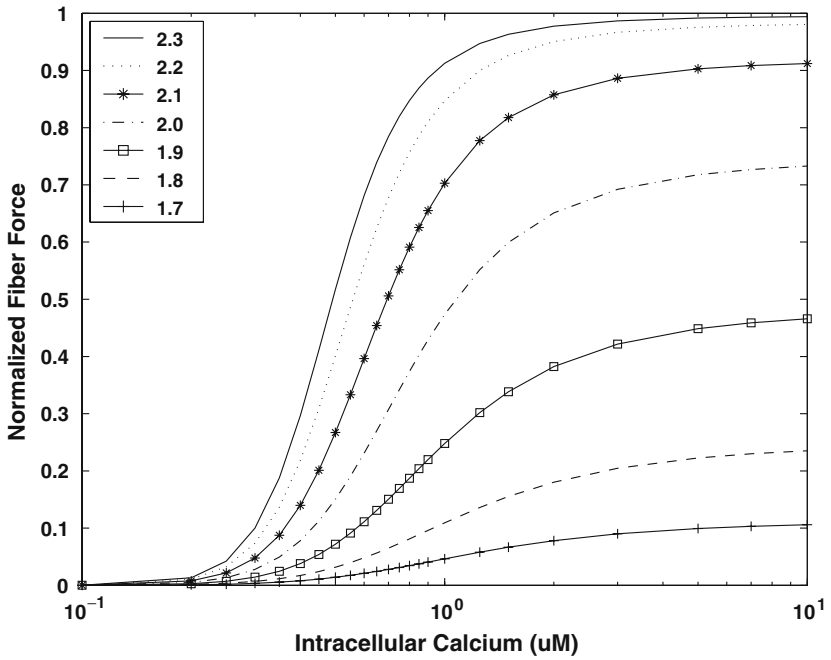

FIGURE 5. Updated steady state force–length relationship of the cardiac contractile mechanism as a function of intracellular free calcium and sarcomere length computed in accordance with Eqs. (10–14).

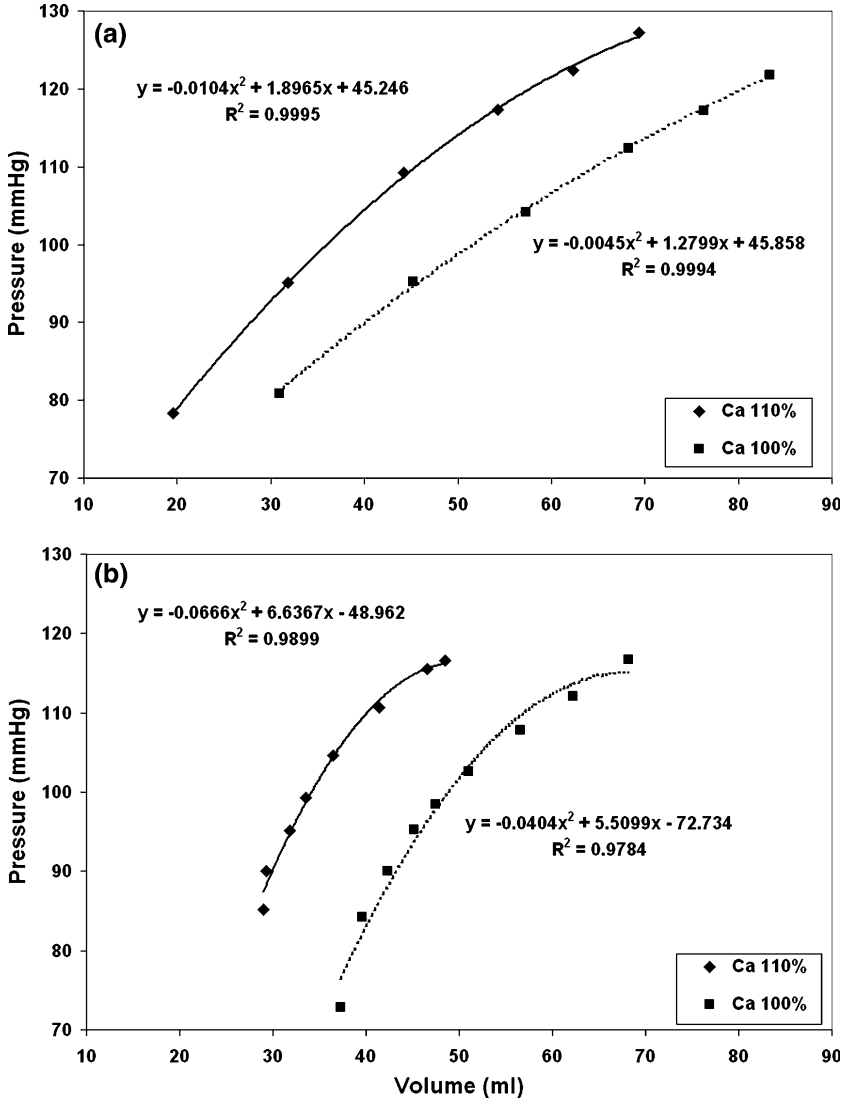

FIGURE 6. Variations in afterload (a) and preload (b) are modeled at different levels of contractility through arterial occlusion and bleeding.

and written, informed consent was obtained before the study from all patients. The average age and weight of the group was 36 ± 8 years and 72 ± 10 kg, respectively. Non-invasive 2-D and Doppler echocardiography examinations were performed using Vivid 7 ultrasound machine (GE Medical Systems, Milwaukee, WI). Echocardiographic images were analyzed for standard indices of systolic and diastolic function. Additional details about experimental protocols and/or data analysis can be found in the works of Notomi *et al.*[17]

Non-invasive and direct measurement of ventricular pressure is not possible, therefore a total of six 25–30 kg mongrel dogs were used to obtain mean values of invasive pressure measurements to supplement non-invasive data obtained in the human experimental model. Detailed information about the treatment of the animals and experimental protocols can be found in the work of Notomi *et al.*[16] The study was approved by the Institutional Animal Research committee and is in compliance with the "Guide for the Care and Use of Laboratory Animals published by the National Institutes of Health." It is well known that systolic blood pressure is fairly constant across species, therefore the pressures were normalized based on the systolic systemic blood pressure. This resulted in a scaling factor of 0.966 for the invasive dog data.

The numerical predictions for all 19 indices of a normal human subject are included in Table 7 and compared to the experimental/clinical values. The histogram in Fig. 7 summarizes the results of the benchmarking. Here and in Table 7, errors are presented as a percentage of the standard deviation in the experimental data for a given cardiovascular index.

TABLE 7. Summary of lumped model validation data: minimum (1) and maximum (2) systemic pressure, minimum (3) and maximum (4) LV pressure, minimum (5) and maximum (6) time derivative of LV pressure, peak left atrial pressure (7), end-diastolic (8) and end-systolic (9) LV volume, stroke volume (10), ejection fraction (11), cardiac output (12), heart rate (13), ejection time (16), peak S/E/A-wave velocities (15–17), time-velocity-integral of the E-wave (18) and E/A-velocity ratio (19).

	Experiment	Model	Error[b]
1. Systemic sys. pressure (mmHg)	110.60 ± 12.73	107.3	0.259 σ
2. Systemic dia. pressure (mmHg)	63.13 ± 8.04	63.9	0.095 σ
3. Max. LV pressure[a] (mmHg)	120.85 ± 8.40	121.8	0.113 σ
4. Min. LV pressure[a] (mmHg)	5.60 ± 2.61	2.26	1.282 σ
5. Maximum dP/dt[a] (mmHg/s)	1249 ± 160	1154	0.592 σ
6. Minimum dP/dt[a] (mmHg/s)	−1221 ± 275	−1030	0.695 σ
7. End-diastolic LAP[a] (mmHg)	11.01 ± 1.16	11.4	0.335 σ
8. LV end-diastolic volume (ml)	103.32 ± 22.51	105.8	0.110 σ
9. LV end-systolic volume (ml)	33.31 ± 8.87	33.9	0.067 σ
10. Stroke volume (ml)	72.38 ± 16.25	71.9	0.087 σ
11. Ejection fraction	67.49 ± 5.32	68.0	0.087 σ
12. Cardiac output (l/min)	4.68 ± 0.95	4.82	0.145 σ
13. Heart rate (1/s)	66.82 ± 10.34	67.00	0.018 σ
14. Ejection time (ms)	283.0 ± 29.0	283.0	0.001 σ
15. Peak S-wave velocity (m/s)	1.04 ± 0.19	1.12	0.407 σ
16. Peak E-wave velocity (m/s)	0.92 ± 0.27	0.92	0.013 σ
17. Peak A-wave velocity (m/s)	0.56 ± 0.10	0.56	0.033 σ
18. TVI of E-wave (cm)	13.68 ± 4.15	12.69	0.239 σ
19. E/A – velocity ratio	1.69 ± 0.48	1.64	0.098 σ

[a] Normalized invasive dog data, used to supplement non-invasive human data.
[b] Difference of the lumped model output compared to experimental data is expressed as a fraction of the experimental standard deviation for each measurement.

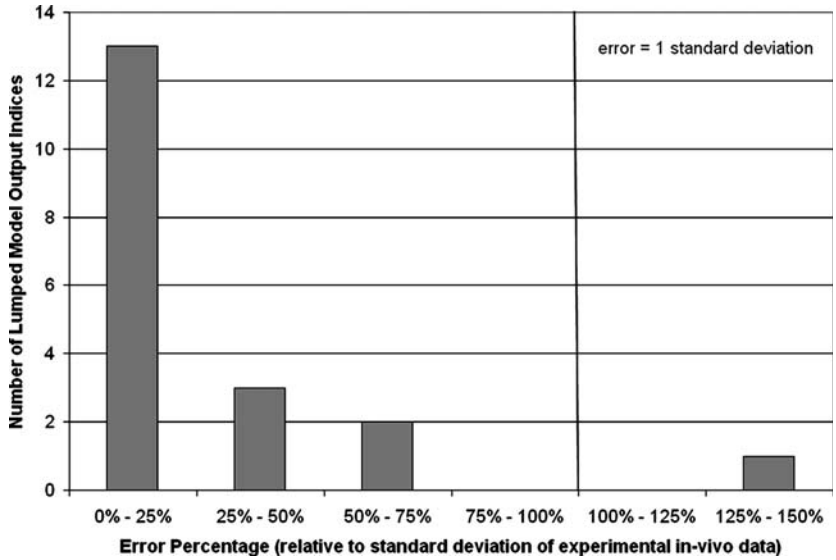

FIGURE 7. Histogram of relative errors in the validation indices: 0–25%: indices 2,3,8,9,10,11,12,13,14,16,17,18,19. 25–50%: indices 1,7,15. 50–75%: indices: 5,6. 125–150%: index 4.

Therefore, in the histogram of Fig. 7, a 100% error in an index indicates that the model prediction for that index is off by 1 standard deviation. Therefore, the histogram shows that 18 out of the 19 predicted physiological indices are within 1 standard deviation and 13 out of 19 indices are within 1/4 standard deviation from the mean experimental values. The mean error is 0.242 standard deviations, while the median is 0.110. Finally, the maximum and minimum errors are 1.282 and 0.001 standard deviations for indices 4 and 14, respectively.

The simulated cardiovascular response of a normal subject as captured by the behavior of key model output variables (such as the pressures, volumes and

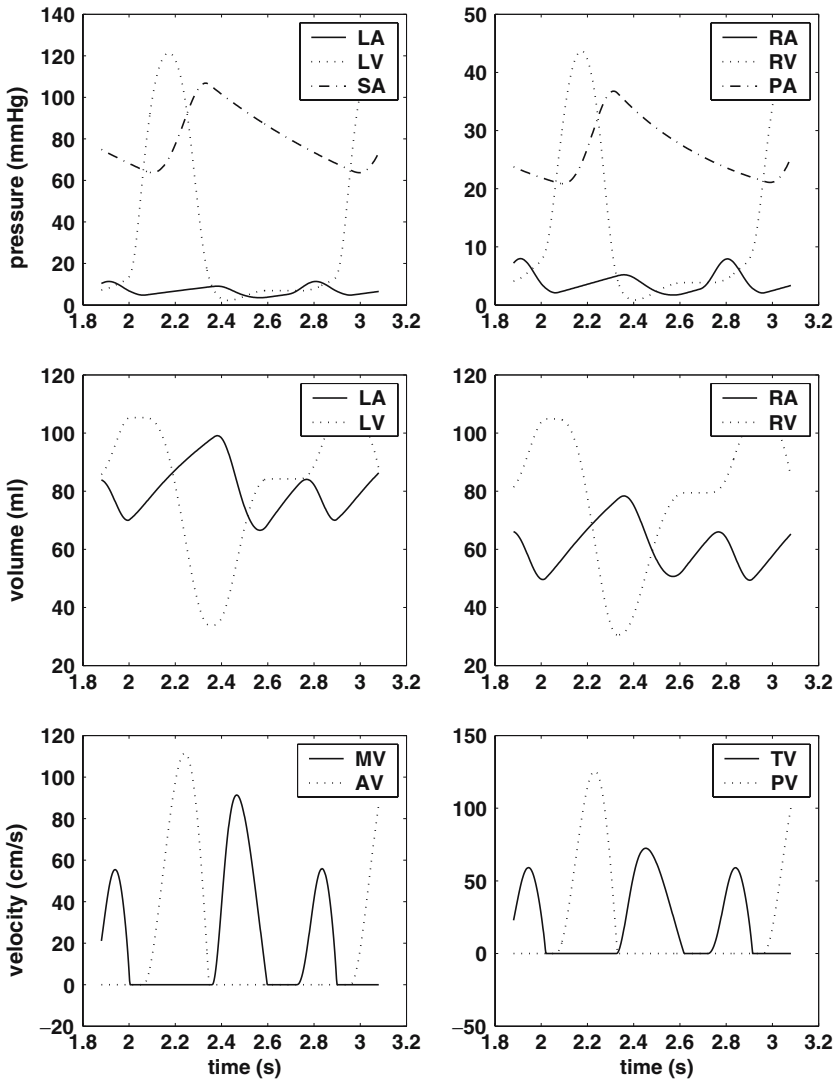

FIGURE 8. Key output pressures, volumes and flow velocities in atria, ventricles, arteries and valves for the baseline model.

flow velocities in the atria, ventricles, arteries, and valves) during one heartbeat are presented in Fig. 8. Briefly, the plots in this figure show that during systole, the increase of the ventricular pressures leads to ejection of the blood from the ventricles through the valves and into the arterial system (S-wave). Upon relaxation of the heart muscle during early diastole, there is a decrease in the ventricular pressures and the filling of the ventricles commences. During this period, flow across the atrio-ventricular valve is biphasic, with characteristic peaks occurring at early diastole and during atrial contraction. The filling associated with early diastole and atrial contraction are known as the E-wave and the A-wave, respectively. If our model did not simulate this biphasic behavior there would be reason for grave concern. The observation of this phenomenon, which represents the corner stone for the analysis of diastolic function, are too numerous to be cited. However, we would like to point to a recent review paper, and a computer modeling study of this phenomenon.[7,32] First the E-wave enters the cavity as a pure consequence of ventricular wall relaxation. Next, additional priming of the ventricle is achieved due to atrial contraction, forcing the blood flow into the ventricle in form of the A-wave. The fiber crossbridge states and the troponin–calcium complex state of the left ventricle during the contracting and relaxing intervals are displayed in Fig. 9. They indicate the formation of force-generating crossbridges (N_1, P_1, P_2, P_3) as calcium leads to unmasking of the binding sites through the formation of the troponin–calcium complex (TCA increases) during systole. Note that as N_1, P_1, P_2, P_3 increase, N_0 will decrease since the sum of all probabilities must equal 1 at all times. Additionally,

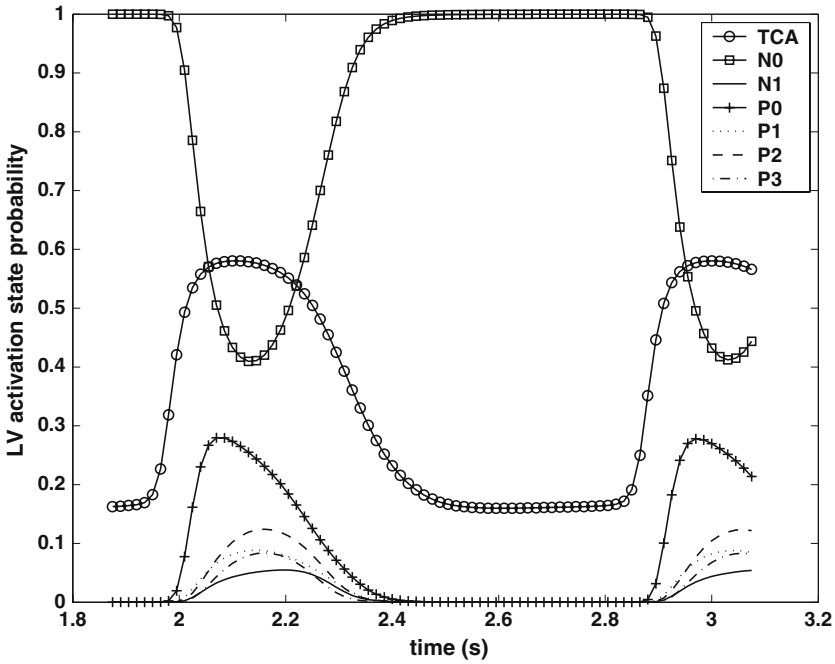

FIGURE 9. Left ventricular crossbridge and troponin-calcium states of the baseline lumped myofilament activation model (see Fig. 3). Note: The frequency of the markers is no reflecting of the time step size.

while P_0 increases during systole, it does not contribute to the generation of force since no crossbridges are bound in this state.

DISCUSSION

In addition to performing three different validation experiments, we will show that the incorporation of the myofilament crossbridging mechanism has indeed improved the validity and physiological fidelity of the present lumped cardiovascular model. Finally, we will provide some examples of how the present model can be used as an efficient and effective hypothesis-testing tool to examine the effect of the different microscale elements of the myofilament crossbridging mechanism on the integrated macroscale performance of the cardiovascular system.

Incorporation of the myofilament activation mechanism results in significant improvements in the physiological fidelity and internal consistency of the present lumped cardiovascular model in comparison to other existing lumped cardiovascular models such as Thomas *et al.*[32], Heldt *et al.*[8] and Lu *et al.*[14] that rely on semi-arbitrary phenomenological systolic stiffness relationships to simulate the ventricular contraction where a pre-determined time-varying stiffness is imposed. While Thomas applied a sinusoidal activation and exponential relaxation, this approach renders an extremely large pressure early in systole, causing complete ejection of the ventricle in 100 ms. Upon complete ejection, the pressure remains elevated due to the lack of the proper length dependency. While Heldt and Lu partially corrected this by a slower linear increase of the stiffness throughout systole,[8–10,14] the lack of the proper dependence of pressure on volume (sarcomere length) and intracellular calcium levels remains abscent.

Figure 10a shows the systolic pressure build up in the left ventricle as predicted by the three cardiovascular models, while Fig. 10b displays a comparison among the corresponding predicted aortic flows. In these figures Model-1 refers to the contraction mechanism as used by Thomas and Model-2 corresponds to the contraction mechanism as implemented by Heldt. Both Model-1 and Model-2 use empirical stiffness relationship for the ventricles. While it is clearly evident from Fig. 10 that the Heldt model outperforms Thomas model as far as the ventricular pressure behavior is concerned, both models produce quite unrealistic aortic blood flow profiles with the predicted peak velocities about a factor 2 higher than observed experimentally. This abnormal behavior is mainly caused by the low inertia of the blood flow in the systemic arteries. One could adjust the parameters in the Heldt model to increase the blood inertia and thus render a more realistic aortic flow profile as shown by Model-3 in Fig. 10b. Unfortunately this parametric adjustment will also cause a 32% increase in peak pressure from 107 mmHg (on Model-2) to 141 mmHg

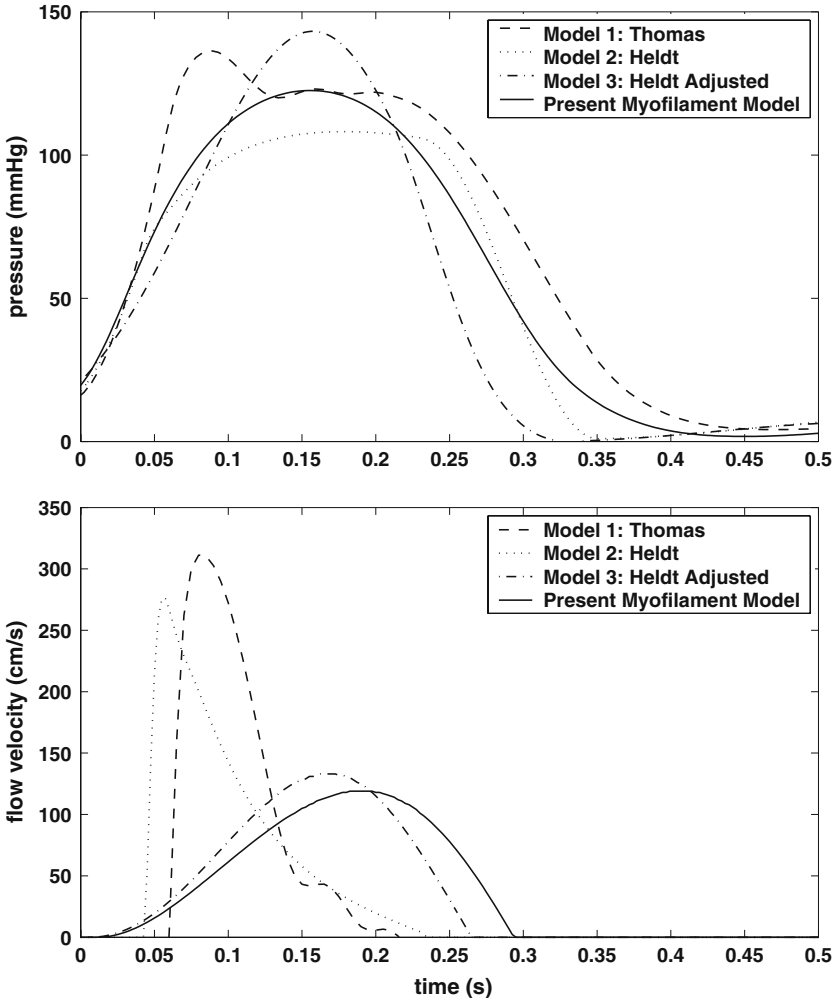

FIGURE 10. Left ventricular pressure and aortic flow computed by the variable compliance lumped models and by the current myofilament activation model.

(on Model-3) as shown in Fig. 10a. When we use our cardiovascular model that simulates the contractile behavior of the ventricles based on the actual myofilament activation mechanism, the pressure and blood flow predictions of our model produce a physiologically plausible and valid behavior (Fig. 10). Thus we conclude that the incorporation of the crossbridging mechanism through a myofilament activation model into the lumped representation of cardiac function as done in the present work will account for the proper dependency of pressure on calcium and fiber stretch (through volume) thus rendering a more realistic pressure and flow behavior as illustrated here.

The current model can easily be used to investigate the impact of several cardiac parameters and/or mechanisms such as calcium binding, crossbridge kinetics, elastic muscle properties, heart rate variations, contractility, etc. For example, in Eq. (9), the contractility can be varied by changing the level of free calcium by varying Ca_{max}. On the other hand, heart rate can be changed by varying the parameters *hr* and Ca_{dur}. While *hr* changes the heart rate, Ca_{dur} alters the duration of systole. Therefore, this model allows the independent variation of systolic and diastolic duration by altering these parameters.

While a detailed discussion of the impact of these mechanisms on cardiac function is beyond the scope of this paper, two cases will be presented to demonstrate the enhanced hypothesis-testing capabilities of the present myofilament-based lumped model. While previous models could not directly alter calcium binding or crossbridge kinetics, the current model has this new capability. The first parametric case study demonstrates how the overall cardiovascular performance is affected by the ventricular calcium levels (Fig. 11) by altering Ca_{max} in Eq. (9). It is clear that the developed pressure, stroke volume and flow velocities decrease as peak calcium level drops causing a loss of ventricular

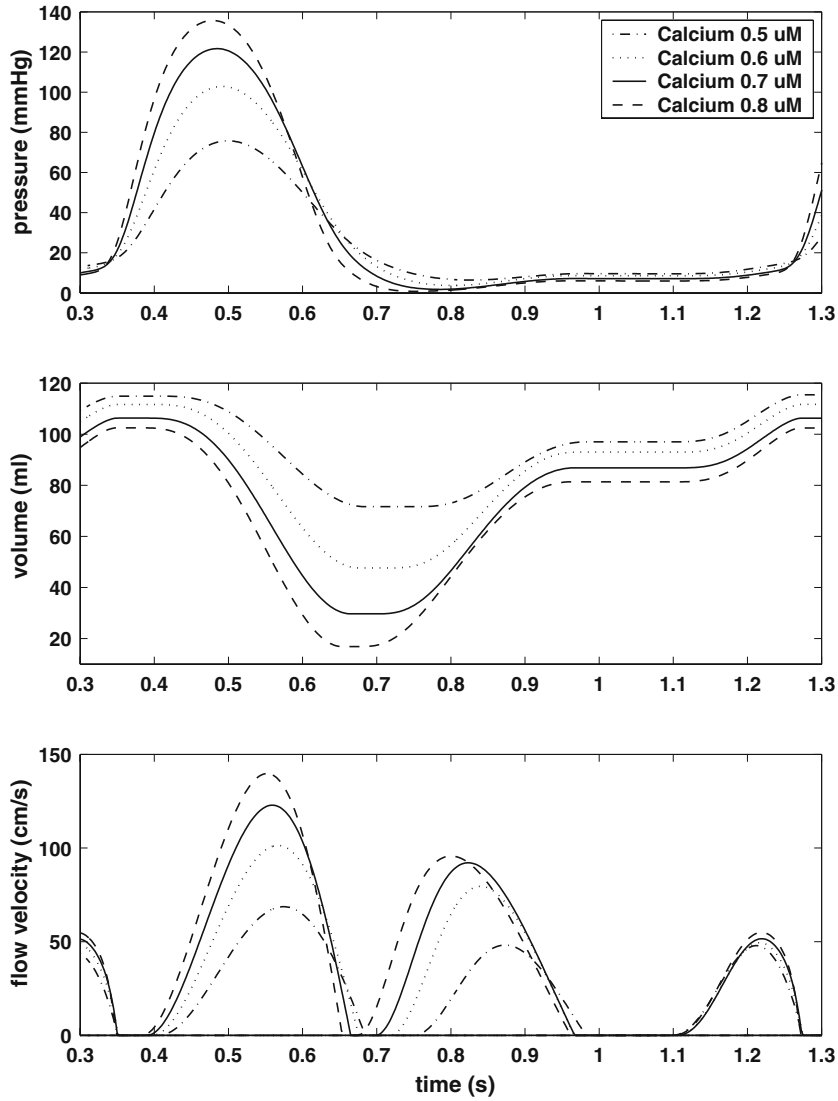

FIGURE 11. Impact of variable peak intracellular calcium level on left ventricular pressure and volume, aortic and mitral flow.

performance. In a second parametric case study, the effect of the crossbridging kinetics rate on the overall cardiovascular performance is examined (Fig. 12) by increasing the rate constant g as defined in Table 6. A reduction in the speed of the crossbridge kinetics leads to a slower pressure rise and slightly reduced peak pressures. As expected, the slowed crossbridging function also delays relaxation, thus decreasing the filling capability of the LV during the E-wave as indicated by the results in Fig. 12.

CONCLUSIONS

In this paper, we have addressed the limitations confronted by many of the lumped cardiovascular models in the literature due to the use of empirically based stiffness relationships for simulating the ventricular contraction. To alleviate this shortcoming we incorporated a comprehensive myofilament activation model into our lumped cardiovascular formulation that can preserve the physiologically dependence of ventricular pressure on fiber sarcomere length and intracellular calcium concentrations, key mechanisms responsible for realistic cardiac function. The resulting cardiovascular model was verified and validated against published benchmark cardiovascular data. It was also shown, through specific case studies, that the present lumped cardiovascular model not only enhances the physiological fidelity of the cardiovascular simulations in comparison to other existing lumped models in the literature, but it also produces a quick response numerical modeling tool that can be used to examine and test various hypotheses concerning the impact of the calcium binding and crossbridging kinetics on the overall performance of the cardiovascular system.

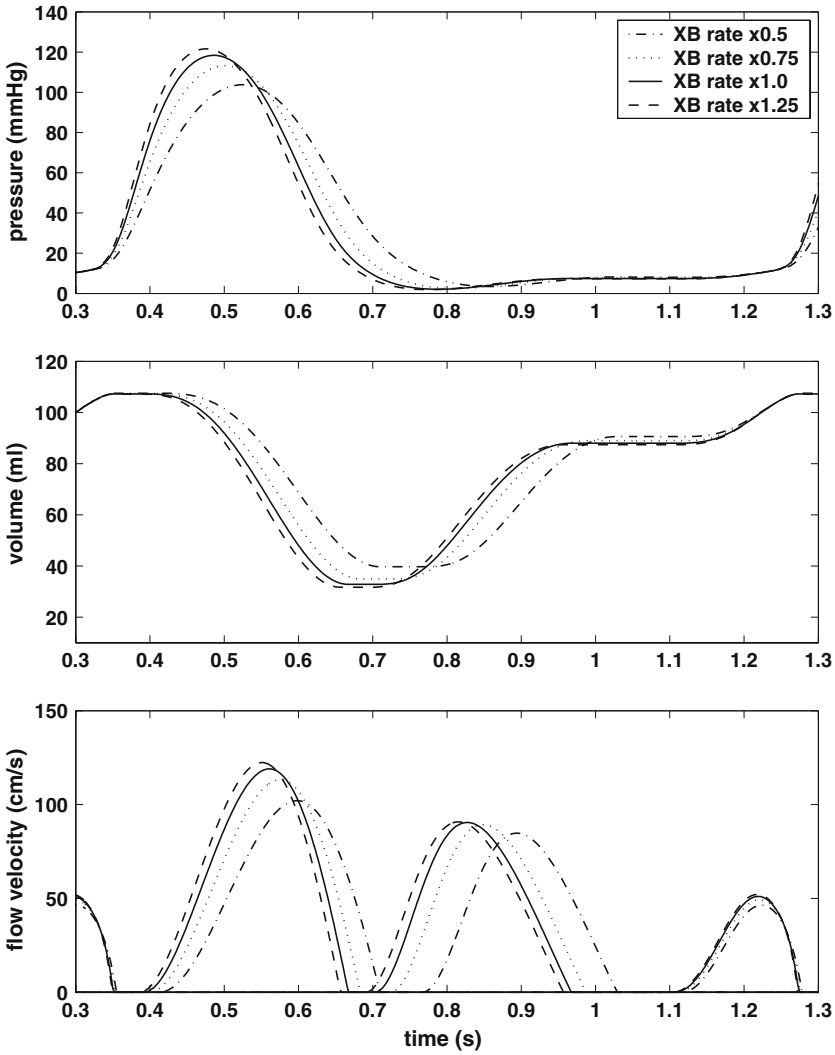

FIGURE 12. Impact of variable crossbridge rate *f*, *g* on left ventricular pressure and volume, aortic and mitral flow.

Several future extensions to the current cardiovascular model are needed to further increase its physiological relevance. First, we intend to develop a more realistic volume–sarcomere length relationship based on numerical data generated by a comprehensive 3D finite element structural model of the heart that includes detailed and anatomically correct heart fiber architecture. We also plan to develop myofilament activation models for both atria. Currently, tissue inertia is not yet included in the lumped models. While this could be justifiable for the vascular system it is less valid for the heart. Finally, vascular models would benefit from a 1D vessel description, rather than 0D lumped analysis, to describe wave propagation effects.[18] Therefore, the effect of cardiac inertia and pressure wave propagations in the main arteries and veins will be assessed in future model developments.

ACKNOWLEDGMENTS

The authors wish to acknowledge Dr Jeremy Rice, IBM Watson Research Center, Yorktown, NY, for the fruitful discussions regarding the myofilament kinetics model. The authors also acknowledge the staff at the Cleveland Clinic Foundation, Cleveland, OH for providing the experimental data, specifically Dr Yuitchi Notomi and Dr Zoran Popovic.

REFERENCES

[1]Bauer, F., M. Jones, T. Shiota, M. S. Firstenberg, J. X. Qin, H. Tsujino, Y. J. Kim, M. Sitges, L. A. Cardon, A. D. Zetts, and J. Thomas. Left ventricular outflow tract mean systolic acceleration as a surrogate for the slope of the left ventricular end-systolic pressure-volume relationship. *J. Am. Coll. Cardiol.* 40(7):1320–1327, 2002.

[2]Burkhoff, D., S. Sugiura, D. Yue, and K. Sagawa. Contractility-dependent curvilinearity of end-systolic pressure-volume relations. *Am. J. Physiol.* 252:H1218–1227, 1987.
[3]Faber, G. M. and Y. Rudy. Action potential and contractility changes in [na(+)](i) overloaded cardiac myocytes: A simulation study. *Biophys. J.* 78(5):2391–2404, 2000.
[4]Firstenberg, M. S., G. Armstrong, N. Greenberg, M. Garcia, and J. Thomas. Deceleration time prolongation in atrial fibrillation: Insights from a numerical model. *J. Am. Coll. Cardiol.* 33(2):449A.
[5]Firstenberg, M. S., D. L. Prior, N. L. Greenberg, S. Wahi, A. Pasquet, M. J. Garcia, and J. Thomas. Effect of cardiac output on mitral valve area in patients with mitral stenosis: Validation and pitfalls of the pressure half-time method. *J. Heart Valve Dis.* 10(1):49–56, 2001.
[6]Formaggia, L., F. Nobile, A. Quarteroni, and A. Veneziani. Multisclae modelling of the circulatory system: A preliminary analysis. *Comput. Visual. Sci.* 2:75–83, 1999.
[7]Garcia, M., J. Thomas, and A. Klein. New doppler echocardiographic applications for the study of diastolic function. *J. Am. Coll. Cardiol.* 32:865–875, 1998.
[8]Heldt, T., E. B. Shim, R. D. Kamm, and R. G. Mark. Computational models of cardiovascular function for analysis of post-flight orthostatic intolerance. *Comput. Cardiol.* 26:213–216, 1999.
[9]Heldt, T., E. B. Shim, R. D. Kamm, and R. G. Mark. Computational model of cardiovascular function during orthostatic stress. *Comput. Cardiol.* 27:777–780, 2000.
[10]Heldt, T., E. B. Shim, R. D. Kamm, and R. G. Mark. Computational modeling of cardiovascular response to orthostatic stress. *J. Appl. Physiol.* 92(3):1239–1254, 2002.
[11]Kass, D., R. Beyar, E. Lankford, M. Heard, W. Maughan, and K. Sagawa. Influence of contractile state on curvilinearity of in situ end-systolic pressure-volume relations. *Circulation* 79:167–178, 1989.
[12]Kentish, J., H. terKeurs, L. Ricciardi, J. Bucx, and M. Noble. Comparisons between the sarcomere length-force relations of intact and skinned trabeculae from the rat right ventricle: Influence of calcium concentrations on these relations. *Circ. Res.* 58:755–768, 1986.
[13]Klein, A. L., R. M. Savage, F. Kahan, R. D. Murray, J. D. Thomas, W. J. Stewart, M. Piedmonte, P. M. McCarthy, and D. M. Cosgrove. Experimental and numerically modeled effects of altered loading conditions on pulmonary venous flow and left atrial pressure in patients with mitral regurgitation. *J. Am. Soc. Echocardiogr.* 10(1):41–51, 1997.
[14]Lu, K., J. Clark, F. Ghorbel, D. Ware, and A. Bidani. A human cardiopulmonary system model applied to the analysis of the valsalva maneuver. *Am. J. Physiol. Heart Circ. Physiol.* 281(6):H2661–2679, 2001.
[15]Mukkamala, R. and R. J. Cohen. A forward model-based validation of cardiovascular system identification. *Am. J. Physiol. Heart Circ. Physiol.* 281(6):H2714–2730, 2001.
[16]Notomi, Y., M. Martin-Miklovic, S. Oryszak, T. Shiota, D. Deserranno, Z. Popovic, N. Greenberg, and J. Thomas. Enhanced ventricular untwisting during exercise: A mechanistic manifestation of elastic recoil described by doppler tissue imaging. *Circulation* 113:2524–2533, 2006.
[17]Notomi, Y., R. Setzer, T. Shiota, M. Martin-Miklovic, J. Weaver, Z. Popovic, H. Yamada, N. Greenberg, R. White, and J. Thomas. Assessment of left ventricular torsional deformation by doppler tissue imaging validation study with tagged magnetic resonance imaging. *Circulation* 111:1141–1147, 2005.
[18]Olufsen, M. A one-dimensional fluid dynamic model of the systemic arteries. *Stud. Health Technol. Inform.* 71:79–97, 2000.
[19]Olufsen, M., and A. Nadim. On deriving lumped models for blood flow and pressure in the systemic arteries. *Math. Biosci. Eng.* 1(1):61–80, 2004.
[20]Olufsen, M., A. Nadim, and L. A. Lipsitz. Dynamics of cerebral blood flow regulation explained using a lumped parameter model. *Am. J. Physiol. Regul. Integr. Comp. Physiol.* 282(2):R611–622, 2002.
[21]Peterson, K. and E. T. Ozawa. Numerical simulation of the influence of gravity and posture on cardiac performance. *Ann. Biomed. Eng.* 30(2):247–259, 2002.
[22]Popovic, Z. B., U. N. Khot, G. M. Novaro, F. Casas, N. L. Greenberg, M. J. Garcia, G. S. Francis, and J. Thomas. Effects of sodium nitroprusside in aortic stenosis associated with severe heart failure: Pressure-volume loop analysis using a numerical model. Am. J. Physiol. Heart Circ. Physiol. 288(1):H416–423, 2005.
[23]Popovic, Z. B., M. Vukovic, N. Greenberg, A. Vlahovic, A. N. Neskovic, and J. Thomas. Comparative value of single-beat load-independent contractility indices in dilated cardiomyopathy and mitral regurgitation. *J. Am. Soc. Echocardiogr.* 16(7):703–711, 2003.
[24]Rice, J. J., M. S. Jafri, and R. L. Winslow. Modeling short-term interval-force relations in cardiac muscle. *Am. J. Physiol.* 278(3):H913–931, 2000.
[25]Rice, J. J., R. L. Winslow, and W. C. Hunter. Comparison of putative cooperative mechanisms in cardiac muscle: Length dependence and dynamic responses. *Am. J. Physiol.* 276(5):H1734–1754, 1999.
[26]Rudy, Y. From genome to physiome: Integrative models of cardiac excitation. *Ann. Biomed. Eng.* 28(8):945–950, 2000.
[27]Schroeder, M. J., V. Phaniraj, S. C. Koenig, R. D. Latham, and D. L. Ewert. The role of arterial elastance in ventricular-arterial coupling in normal gravity and altered acceleration environments. *Aviat. Space Environ. Med.* 72(1): 1–7, 2001.
[28]Segers, P., N. Stergiopulos, J. J. Schreuder, B. E. Westerhof, and N. Westerhof. Left ventricular wall stress normalization in chronic pressure-overloaded heart: A mathematical model study. *Am. J. Physiol. Heart Circ. Physiol.* 279(3):H1120–1127, 2000.
[29]Shaw, R. M. and Y. Rudy. Ionic mechanisms of propagation in cardiac tissue. Roles of the sodium and l-type calcium currents during reduced excitability and decreased gap junction coupling. *Circ. Res.* 81(5):727–741, 1997.
[30]Soans, D., G. Szabo, C. Bolind, and L Waite. A variable valve area, lumped parameter model of left ventricular filling. *Biomed. Sci. Instrum.* 38:483–488, 2002.
[31]Thomas, J. D., M. J. Garcia, and N. L. Greenberg. Application of color doppler m-mode echocardiography in the assessment of ventricular diastolic function: Potential for quantitative analysis. *Heart Vessels* 12:135–137, 1997.
[32]Thomas, J. D., J. Zhou, N. Greenberg, G. Bibawy, P. M. McCarthy, and P. M. Vandervoort. Physical and physiological determinants of pulmonary venous flow: Numerical analysis. *Am. J. Physiol.* 272(5 Pt 2):H2453–2465, 1997.
[33]Waite, L., S. Schulz, G. Szabo, and C. F. Vahl. A lumped parameter model of left ventricular filling-pressure waveforms. *Biomed. Sci. Instrum.* 36:75–80, 2000.
[34]White, R. J. Weightlessness and the human body. *Sci. Am.* 279(3):58–63, 1998.

[35]Wijkstra, H., and H. B. Boom. Deactivation in the rabbit left ventricle induced by constant ejection flow. *IEEE Trans. Biomed. Eng*. 36(11):1112–1123, 1989.

[36]Ye, G. F., T. W. Moore, and D. Jaron. Incorporating vessel taper and compliance properties in Navier-Stokes based blood flow models. *Ann. Biomed. Eng*. 21(2):97–406, 1993.

[37]Yoshigi, M., G. D. Knott, and B. B. Keller. Lumped parameter estimation for the embryonic chick vascular system: A time-domain approach using mlab. *Comput. Methods. Programs. Biomed.* 63(1):29–41, 2000.